

Bubble-Point Measurements and Modeling of Binary Mixtures of Linear Siloxanes

Luuc Keulen,^{†,§} Elisabeth Mansfield,^{*,‡} Ian H. Bell,[‡] Andrea Spinelli,[¶] and
Alberto Guardone[†]

[†]*Department of Aerospace Science & Technology, Politecnico di Milano, Via La Masa 35, 20156
Milano, Italy*

[‡]*Applied Chemicals and Materials Division, National Institute of Standards and Technology,
Boulder, CO 80305, United States of America*

[¶]*Energy Department, Politecnico di Milano, Via Lambruschini 4, 20156 Milano, Italy*

[§]*Current affiliation: ASML, De Run 6501, 5504DR Veldhoven, The Netherlands*

E-mail: elisabeth.mansfield@nist.gov

Abstract

The bubble-point pressures of three binary mixtures of linear siloxanes have been measured. The binary mixtures consist of hexamethyldisiloxane (MM) which is mixed with either octamethyltrisiloxane (MDM), decamethyltetrasiloxane (MD₂M), and dodecamethylpentasiloxane (MD₃M). For each mixture, three compositions were measured where MM was present in approximately 25 mol%, 50 mol%, and 75 mol%. The bubble-point pressures were measured over a temperature range of 270 K to 380 K for all mixtures. Large uncertainties are

*Commercial equipment, instruments, or materials are identified only in order to adequately specify certain procedures. In no case does such identification imply recommendation or endorsement by the National Institute of Standards and Technology, nor does it imply that the products identified are necessarily the best available for the purpose. Contribution of the National Institute of Standards and Technology, not subject to copyright in the US.

observed for the lower temperatures (below 320 K) due to non-condensable impurities. A detailed analysis is performed to determine the effect of non-condensable gases on the measured bubble-point pressure data. The newly obtained bubble-point pressure data is used to determine new binary interaction parameters for the multicomponent Helmholtz energy model. The data used for the fitting of the binary interaction parameters are weighted by the relative uncertainty, this ensures that data points with high uncertainty contribute less to the final binary interaction parameter. In this work, a description of the experimental apparatus and measurement procedure is given, as well as the measured bubble-point pressure data and newly obtained binary interaction parameters.

1 Introduction

The need for high quality thermophysical property data with thoroughly assessed sources of uncertainty is of great importance¹. The data measured are important for the development of high accuracy equations of state for the prediction of the thermophysical properties of a fluid over large ranges of temperature and pressure. In turn, the predicted properties can be used for efficient design of power cycles as well as other industrial processes such as chemical manufacturing and air conditioning. For the development of a reliable equation of state, vapor-liquid equilibrium (VLE) and homogeneous density data are required. To obtain well established calculation of caloric properties, isobaric heat capacity, and speed of sound data are required.

As mentioned VLE is a key thermophysical property and accurate VLE data is necessary for model development of equations of state to predict thermophysical properties. Knowledge about the phase change of pure fluids and mixtures is of paramount importance for the design and operation of industrial and research applications. Knowing the temperature and pressure at which these changes take place allow for more efficient use of the fluid. To determine phase behavior of pure fluids, temperature and pressure need to be measured, for mixtures it is also necessary to know the composition of the mixture. The two main methods to determine VLE for mixtures are the analytical and the synthetic method. They differ on how the composition of the equilibrium phases

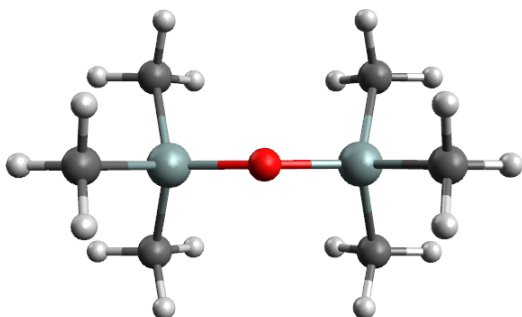
are determined. The analytical method involves the analytical determination of the composition of the coexisting phases. In the analytical method it is not necessary to exactly know the overall composition of the mixture when the fluid is loaded into the equilibrium cell. The composition of the coexisting phases of the mixture is analyzed with sampling using chemical analysis or without sampling by using physiochemical methods of analysis inside the equilibrium cell. For the synthetic method, the mixture is prepared with a precisely known composition and then the prepared mixture is loaded into the equilibrium cell and the properties are measured in the equilibrium state. An extensive review about the analytical and synthetic methods for the measurements of VLE data is given by Fonseca et al.².

The equipment for the bubble-point measurements used in this work is based on the synthetic method, where a precisely known mixture composition is made gravimetrically offline. The synthetic method yields pressure, temperature, and liquid composition data. Which in comparison with analytical instrumentation returns pressure, temperature, liquid and vapor composition data. The synthetic methods allows for more simplistic equipment design because the composition does not have to be determined. Simpler equipment allows for the sources of uncertainty to be identified and accounted for in a way that analytical methods do not. By eliminating sampling valves and composition determining instrumentation (e.g. gas chromatography), which most analytical methods use^{2,3}, the uncertainty in potential composition changes that occur when volume is removed from the system are eliminated. In addition, a double substitution weighing design to determine composition ensures that the composition of the mixture is well known, extreme care in calibration of pressure transducers is accomplished with a dead weight pressure balance, and temperatures are calibrated using a three point calibration for highest precision⁴. These measures ensure that the sources of uncertainty are well characterized.

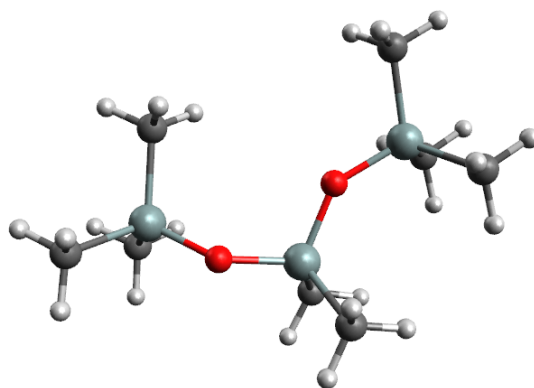
In this work bubble-point pressure measurements of binary mixtures of linear siloxane fluids are conducted, the molecular structure of the linear siloxanes measure is shown in Fig. 1. The binary mixtures consist of hexamethyldisiloxane (MM) shown in Fig. 1a which is mixed with either octamethyltrisiloxane (MDM), decamethyltetrasiloxane (MD₂M), and dodecamethylpentasiloxane

(MD₃M), the molecular structures are shown in Figs. 1b to 1d respectively. The obtained bubble-point pressure data are used to improve the current equation of state models for the binary mixtures of linear siloxanes by modeling new mixture parameters. The measurements and modeling are performed at the National Institute of Standards and Technology. Pure siloxane working fluids are already prominent, successful working fluids for instance Organic Rankine Cycles (ORCs). Mixtures of siloxanes are promising working fluids for ORCs⁵. The use of ORCs as power cycles has increased significantly the last few decades and is now a widely used technology for small to medium power generation. They are used in many different applications, from industrial waste heat recovery to renewable energy application, such as solar, biomass and geothermal energy⁶⁻⁹. For binary mixtures of linear siloxane only one data set exists, which is conducted by Abbas¹⁰, and no binary mixture parameters have been modeled for these mixtures so far, prompting the need for additional measurements and mixture modeling.

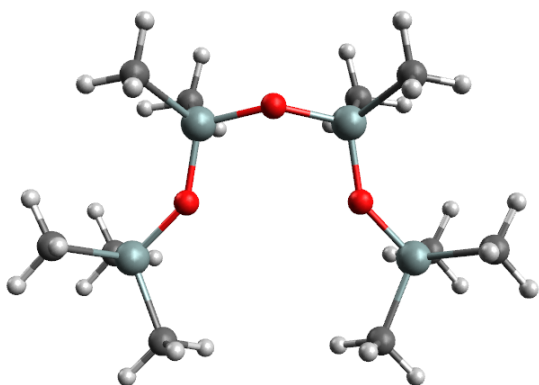
The structure of this work is as follows. Firstly, Section 2 describes the linear siloxane fluids measured and modeled in this work. In Section 3 the details of the bubble-point pressure measurement equipment are given, describing the various components of the apparatus and their specifications. Subsequently the mixture preparation is elaborated as well as the procedure for the measurement of the bubble-point pressure in Section 4. The data analysis consisting of the analysis of the vapor quality in the equilibrium cell and the thorough uncertainty analysis is discussed in Section 5. The results and discussion of the bubble-point measurements are presented in Section 6 and in addition an analysis of the impact of air impurity on the bubble-point pressure is conducted. Section 7 addresses the modeling of new binary interaction parameters for the Helmholtz energy model employing the measured bubble-point pressures. Finally, in Section 8 concluding remarks and recommendations for future research are given.



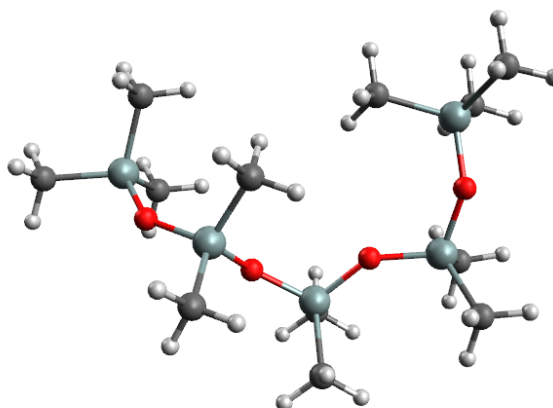
(a) Hexamethyldisiloxane.



(b) Octamethyltrisiloxane.



(c) Decamethyltetrasiloxane.



(d) Dodecamethylpentasiloxane.

Figure 1: Molecular structure of linear siloxanes measured in this work¹¹. a) Hexamethyldisiloxane, b) Octamethyltrisiloxane, c) Decamethyltetrasiloxane, and d) Dodecamethylpentasiloxane.

2 Materials

The fluids were obtained from commercial sources and used without further purification, the stated manufacturer purity is listed in Table 1. The purity of the fluids were measured through chemical analysis and these purities are reported in Table 1.

Table 1: Measured and manufacturer determined purity of the components.

Chemical	Chemical formula	CAS number	Manufacturer	HRGC - MS ¹
MM	C ₆ H ₁₈ OSi ₂	107-46-0	> 99.4%	99.75 %
MDM	C ₈ H ₂₄ O ₂ Si ₃	107-51-7	> 99.7%	99.97 %
MD ₂ M	C ₁₀ H ₃₀ O ₃ Si ₄	141-62-8	> 99.3%	99.81 %
MD ₃ M	C ₁₂ H ₃₆ O ₄ Si ₅	141-63-9	> 98.0%	99.80 %

The purity of the fluids were determined through in house laboratory chemical analysis; for this purpose samples were taken and analyzed by High Resolution Gas Chromatography (HRGC) by using a gas chromatograph equipped with capillary columns attached to a Mass Spectrometer (MS). Spectral peaks were interpreted with guidance from the NIST/EPA/NIH Mass Spectral Database¹² and the Wiley Registry of Mass Spectral Data¹³. The area of the spectral peaks with respect to the largest area peak is obtained and the relative peak percentage is calculated to determine the purity. Because the chemical analysis purities are given in relative percentage between the detected components, this percentage does not correspond to the molar or mass fraction of each component. The chemical analysis allowed for the quali-quantitative analysis of the fluids purity.

3 Experimental apparatus

The schematic design of the experimental apparatus is shown in Fig. 2. The apparatus design is based on an previous apparatus at the National Institute of Standards and Technology¹⁴. The heart of the apparatus is the equilibrium cell constructed of stainless steel and is of high thermal mass to maintain stable temperature control for the duration of the measurement. Temperature is measured using a standard platinum resistance thermometer (SPRT) and pressure is measured

¹High Resolution Gas Chromatography - Mass Spectrometry

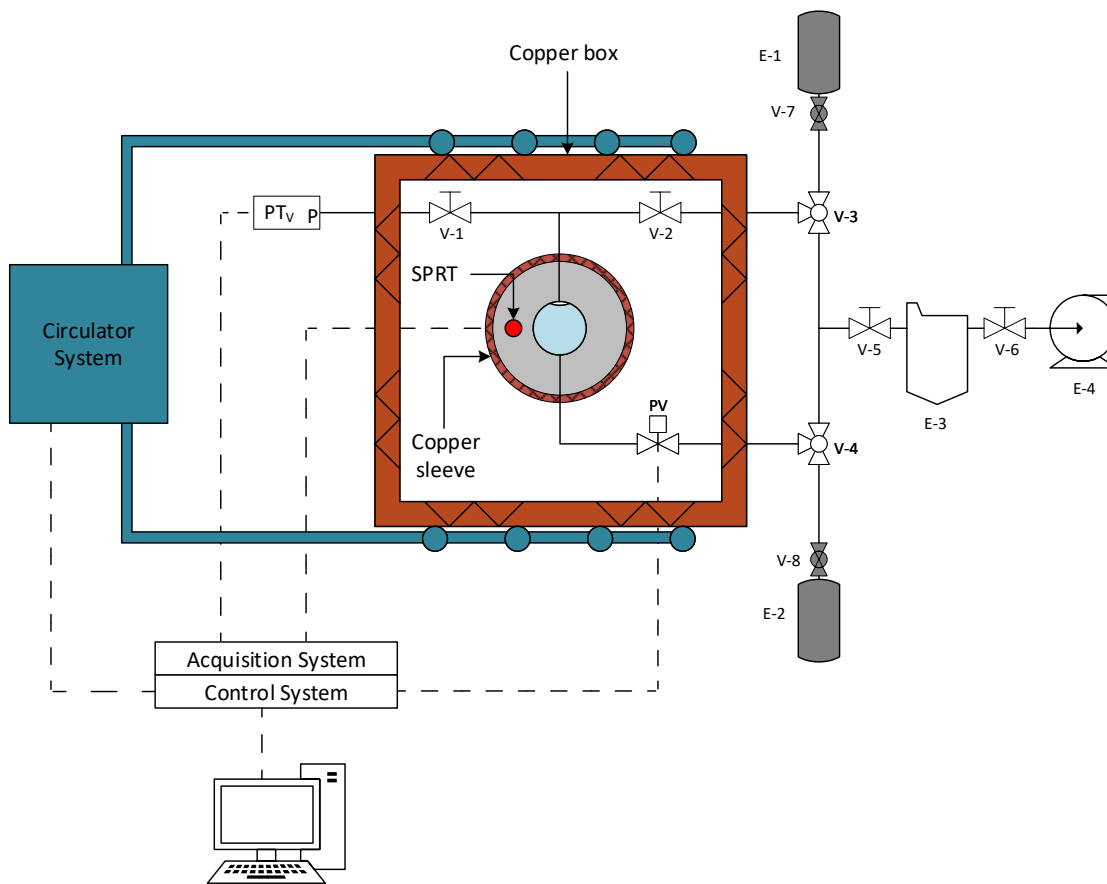


Figure 2: Schematic diagram of the Vapor-Liquid equilibrium experimental apparatus: pressure transducer vapor side (PT_V), standard platinum resistance thermometer (SPRT), valves (V), pneumatic valve (PV), sample vessel (E-1), waste vessel (E-2), cold trap (E-3), vacuum pump (E-4).

using a calibrated oscillating quartz pressure transducer maintained at a constant temperature of 313 K.

Heating and cooling is achieved through a two-stage system; the first stage is formed by a copper sleeve immediately around the equilibrium cell providing direct heat to the cell during the temperature ramp and trim heating once at the equilibrium temperature up to 380 K. The second stage of the thermostat region consists of a copper box around the equilibrium cell and also contains the majority of the valves and tubing. The copper box provides consistent heating throughout the measurement to ensure temperature effects from the room do not influence the cell during the measurement. Cooling also occurs at the copper box by circulating cooling fluid from the circulator system to reach temperatures down to 265 K.

3.1 Equilibrium cell

The cylindrical equilibrium cell houses the fluid undergoing the testing. The cell is constructed from 316 stainless steel with an internal diameter of 22.2 mm, outer diameter of 62.8 mm, and an internal length of 76.2 mm; the internal volume is approximately 30 ml. At each end, the cell has sapphire windows with a thickness of 12.8 mm and diameter of 31.6 mm so that the liquid level in the cell can be observed and controlled as shown in Fig. 3. The windows are held in place by bolted flanges and sealed with fiberglass impregnated polytetrafluoroethylene (PTFE) gaskets on both sides of the windows. The cell has four ports for 3.175 mm outer diameter tubing connections to valves and the rest of the system.

3.2 Thermostat system

The first stage in the thermostat system is a 5.0 mm thick copper sleeve immediately around the equilibrium cell. Flexible heaters on the copper sleeve allow for indirect heating of the equilibrium cell. The copper sleeve is maintained at the equilibrium set point temperature of the equilibrium cell.

The second stage in the thermostat system region is a copper box. The box is centered around

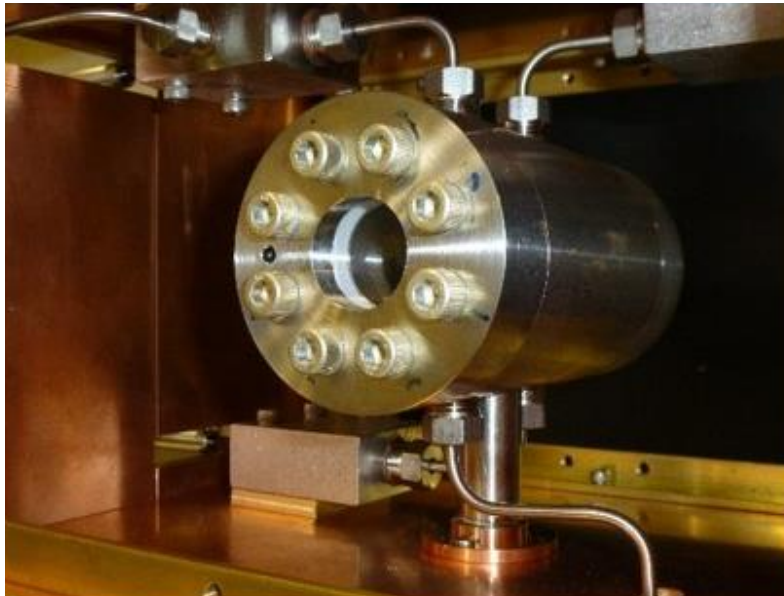


Figure 3: Equilibrium cell Vapor-Liquid equilibrium experimental apparatus.

the equilibrium cell and has an overall dimensions of $216.0 \text{ mm} \times 178.0 \text{ mm} \times 140.0 \text{ mm}$ and a wall thickness of 6.35 mm . The box is fitted with flexible heaters as well as cooling coils for temperature control of the system. These heaters are heated by providing electrical power during the heating phase and are controlled to trim heating during the equilibrium phase to maintain a constant temperature.

For cooling, 9.5 mm outer diameter copper tubing has been brazed to the top and bottom of the box in a serpentine configuration for circulation of cooling fluid when the system is running at sub-ambient temperatures. The cooling fluid is a mixture propylene glycol and water and is circulated by a pump embedded in the thermal bath.

The copper box is contained in a framed aluminum box. Both the inside of the copper box and the area between the copper and aluminum boxes are filled with mineral wool insulation. The thermostat system is capable of maintaining the equilibrium set-point temperature (as measured by the main SPRT) within $\pm 5 \text{ mK}$.

3.3 Temperature system

Temperature is measured in the wall of the equilibrium cell using a SPRT. The SPRT was calibrated using the fixed-point cells and the procedures outlined by Preston-Thomas⁴. Calibration points are a gallium melting point cell (302.9146 K) and the freezing point cell of indium (429.7485 K), each kept in their own thermostat or furnace. A water triple-point cell (273.16 K) was used as the final temperature calibration. The uncertainty for the temperature standards ranges from 0.2 mK to 2 mK. All calibration points were measured using the multimeter used within the VLE apparatus. The copper box is maintained at ± 3 K below the equilibrium set-point temperature of the equilibrium cell. Because an accurate temperature measurement is not necessary for the copper box, the temperature is monitored with a ceramic resistance temperature detector (RTD) fitted to the inner portion of the copper box and recorded using a multimeter equipped with a scanning card.

3.4 Pressure system

The pressure of the system is measured by using an oscillating quartz-crystal pressure transducer (PT) in the vapor phase in the equilibrium cell. The PT has a range up to 700 kPa and is located outside the copper box 50 mm above the center of the equilibrium in an aluminum housing. The PT is calibrated with a NIST-traceable dead-weight pressure gauge at 313 K. The manufacturer stated the uncertainty as 0.01% of full range, equating to 0.07 kPa. However, with regular calibration and maintaining the PT at a constant temperature (313 K) during pressure measurements, the uncertainty can be reduced to 0.005% of the full range, equating to 0.035 kPa. As a conservative estimate of pressure uncertainty, the manufacturer's recommendation of 0.01% of the full range is used. The pressure was monitored using transducer readouts coupled with the acquisition system and computer.

The PT is kept at a constant temperature of 313 K during all pressure measurements of the experiment. The heating of the PT is done via flexible heaters on the aluminum box housing the PT. The temperature control of the aluminum housing is achieved with a commercially available controller that monitors the temperature using a type K thermocouple.

3.5 Additional equipment

All tubing between the equilibrium cell, valves, and pressure transducer is 3.2 mm outer diameter stainless steel tubing. The sample is loaded into the equilibrium cell from the stainless steel sample cylinder E-1 of 300 ml coupled to the apparatus. The three-way valve V-3 was placed between the sample loading tube and the system in order to be able to isolate the loading area and evacuate all the tubing and the equilibrium cell. The valve V-2 between the three-way valve V-3 and the equilibrium cell is used to load the sample through the top port of the equilibrium cell. The port on the bottom of the equilibrium cell is coupled to a pneumatic valve PV. The pneumatic valve PV is used to evacuate fluid from the equilibrium cell, to regulate the liquid level, and acts as a safety mechanism to prevent over-pressurizing the system. The pneumatic valve PV is controlled via the computer and the opening time of the pneumatic valve PV can be varied. The outlet of the pneumatic valve PV is connected to a three-way valve V-4 which is then connected to a stainless steel cylinder for waste collection E-2 and the vacuum system consisting of the cold trap E-3 and vacuum pump E-4. The system can be isolated from the vacuum system through valve V-5. The vapor phase pressure transducer PT_v is connected with the equilibrium cell through valve V-1.

All tubing and connections are verified to be sealed with pressurized helium and under vacuum. The vacuum pump equipped with a cold trap is used to evacuate the entire system, including the equilibrium cell, tubing and waste cylinder prior to loading the sample.

3.6 Electronics and acquisition system

The apparatus data acquisition program monitors the temperature and pressure, controls the power supply for heating, the circulator for cooling, and the pneumatic valve. The program runs an automated loop of a temperature queue set for the test.

Below 300 K, the temperature control program turns on and set the temperature of the circulator, and the heating system is used to shim the temperature and provide stability. Above 300 K, the equilibrium cell is heated by the heating system. The temperature control program is a Proportional-Integral-Derivative (PID) routine. Two independent PID controllers are used for con-

trolling the two heating stages, i.e. the copper sleeve and the copper box. In a feedback loop, the PID controller determines the necessary voltage to reach and then maintain the set-point temperature. The voltage information is transmitted via an IEEE 488 interface to programmable power supplies that power the heaters of the copper sleeve and copper box.

The pressure transducer data is monitored through an USB-to-Serial connection. Calibrations are used to update the pressure transducer coefficients prior to utilizing the pressure transducer in the equilibrium apparatus. The SPRT and RTD are monitored using a multimeter with a scanning card. Temperature and pressure measurements are recorded every 90 seconds.

Equilibrium in the cell is determined by monitoring the temperature. Once sufficient stability is achieved, as defined by tunable convergence criteria, the system is maintained at the equilibrium temperature for 8 hours to ensure equilibrium between the liquid and gas phase is achieved. After the 8 hours equilibrium hold the bubble-point pressure and temperature data is collected for 15 minutes. The collected 15 minutes of bubble-point pressure and temperature data are averaged and recorded as one equilibrium point. After the data collection is completed the software sets the next set-point temperature in the queue and starts heating and the measurement process begins again.

Several safety checks for the system are incorporated into the software. Temperature and pressure limits are set to initiate a safety stop on the system if the system temperature exceeds 410 K or if the pressure reaches 670 kPa; pressures above 670 kPa can damage the pressure transducer. If the safety limits are reached, all heating of the system is stopped. The system could potentially over-pressurize if the vapor phase bubble disappears and a compressed liquid is formed inside the equilibrium cell. If this happens, the pressure rise will trigger the program to open the pneumatic valve and release a small volume of sample into the waste line. If the pneumatic valve cannot compensate the pressure increase by releasing liquid, a safety stop is initiated and all heating ceases. The pneumatic valve can also be triggered manually through the software to control the bubble size.

4 Measurement procedure

The measurement procedure is divided into two parts: the preparation of the mixture sample and the bubble point measurement.

4.1 Mixture preparation

The mixtures are prepared gravimetrically in sealed 300 ml stainless steel cylinders. Mixtures are prepared with the goal of filling the sample cylinder with approximately 280 ml of liquid at the target composition, at ambient temperature. After the weighing of the empty cylinder, the first component is added to the cylinder. In this work MM is always loaded as the first component. After the first component is loaded, the vessel is closed and the vapor space is degassed by freezing the fluid in liquid nitrogen and evacuating the head space. After evacuation, the cylinder is heated to drive impurities in the liquid into the vapor space. This cycle of freezing/evacuating/heating/thawing is repeated at least three times and a maximum of fifteen times, depending on each sample to allow for a complete degassing of the sample. After completion of degassing the cylinder is weighted to determine the amount of fluid of the first component. Next, the second component is added into the vessel and the cycle of freezing/evacuating/heating/thawing is repeated and the completed mixture is weighted to determine the total amount of the second component.

The weighing of the sample cylinder is conducted following the double substitution weighing design of Harris and Torres¹⁵. A balance with a precision of 0.1 mg is used in the preparation of the mixture. Measurement of the mass of the empty cylinder and each component consists of weighing four masses: (1) a reference cylinder of approximately the same mass and volume as the empty sample cylinder, (2) the sample cylinder, (3) the sample cylinder plus a 20 g sensitivity weight, and (4) the reference cylinder plus the 20 g sensitivity weight. This weighing sequence is repeated four times for each mass determination. The density of ambient air is calculated based on measurements of temperature, pressure, and relative humidity, and the weighings are corrected for the effects of air buoyancy¹⁶. The uncertainty of the measured mixture composition is discussed

in detail in Section 5.2.

4.2 Bubble-Point measurement

The system is evacuated and then cooled to 265 K. The sample cylinder is heated for 15 minutes to an estimated temperature of 313 K. The heating is performed to promote convection mixing in the vessel and ensure the sample is adequately mixed and homogenized prior to loading into the equilibrium cell which is under vacuum. The sample is loaded by opening the sample valve and allowing the liquid mixture sample to flow gravimetrically and by the temperature difference into the equilibrium cell. Because the loading volume is very limited and the linear siloxanes mixtures have a very low vapor pressure, the sample remains in the liquid phase during the loading procedure, in this way bubble point measurements on a sample of fixed composition are obtained. The equilibrium cell is filled completely, with the exception of a small vapor space called the "bubble" at the top of the cell. The bubble is kept as small as possible to ensure the vapor composition and bulk liquid composition are equivalent when the system reaches equilibrium. Prior to loading, the vacuum pressure is recorded and measured pressures have been adjusted to reflect any offset. Due to the low vapor pressure of siloxanes, a small contamination of air can have a large impact on the measurement as elaborated in Section 6.1. If necessary, the fluid can be degassed in situ by applying vacuum to the vapor phase of the equilibrium cell. The change in composition of the mixtures by applying vacuum to the vapor space is elaborated in Section 6.2.

Pressure measurements are recorded in the range between 270 K and 380 K, with increments of $\Delta T = 5$ K or $\Delta T = 10$ K. As the cell temperature is increased the liquid inside expands and it is necessary to periodically release a small amount of liquid via the pneumatic valve to maintain a vapor space on the top of the cell. When and in what amount liquid needs to be released depends on the sample and it is monitored and determined by the operator by checking the vapor space after every temperature increase.

Under this measurement protocol, attempts are made to ensure that the most accurate bubble points of the sample are measured, though several assumptions are made. These assumptions

include: (i) the liquid composition in the cell is equal to the bulk composition of the mixture in the sample bottle and no composition change occurs during filling¹⁴, (ii) during degassing of the equilibrium cell vapor space no change of the liquid bulk composition occurs, and (iii) by loading the equilibrium almost full of liquid, leaving only a very small vapor space, the pressure of the vapor phase equals the bubble-point pressure of the liquid composition at a given temperature; this is analyzed in Section 5.1.

5 Data Analysis

All processing of the data and uncertainty calculations are performed using an in-house analysis software. Modeling of the data analysis is performed using the thermodynamic model implemented in computer program REFPROP¹⁷. Due to the absence of binary interaction parameters for the Helmholtz energy equation of state for the mixture measured in this work the Peng-Robinson equation of state^{18,19} from REFPROP is used for the data analysis.

5.1 Vapor quality equilibrium cell

The vapor quality in the equilibrium cell is determined by an analysis of the vapor bubble and the use of the void fraction ϵ to characterize the two-phase regions. The analysis of the vapor quality is done to evaluate the assumption that the measurements are performed at the bubble point. This analysis provides an indication of the change in vapor quality with vapor bubble size and temperature increase through estimated properties using the thermodynamic model.

The vapor quality, q , is determined following the procedure described in the supplementary material. The determination of the vapor quality is based on the void fraction, which calculation is purely geometric in nature. The change in vapor quality with increasing vapor bubble size is shown in Fig. 4 for mixtures of MM with MDM, MD₂M, and MD₃M. The vapor quality increases with larger vapor bubble size; mixtures with a larger fraction of MM show a steeper increase of the vapor quality. The vapor quality increase is very small; for all mixtures the vapor quality is less

than 1×10^{-4} when the vapor phase occupies half of the cell.

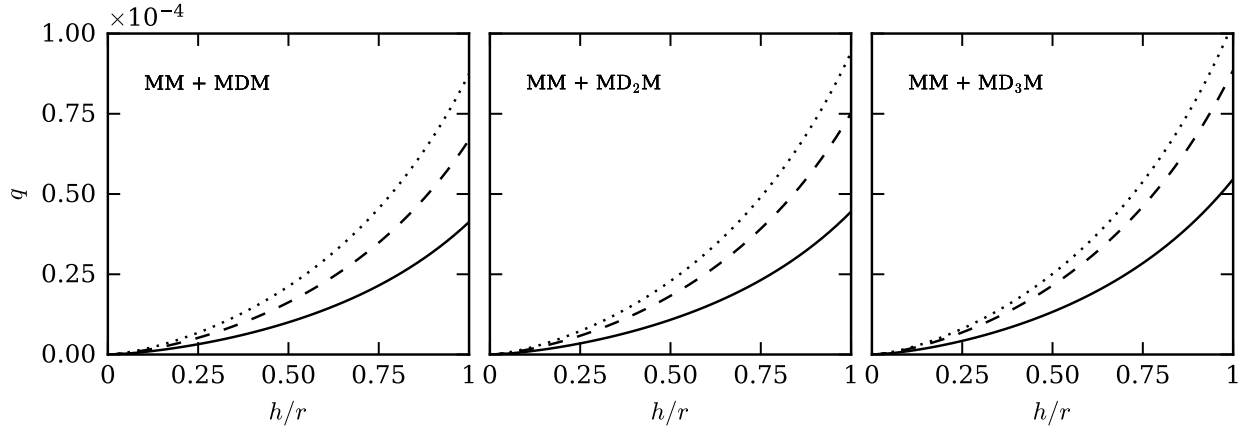


Figure 4: Vapor quality determination on three compositions of each mixture of MM with MDM (left figure), MD₂M (middle figure), and MD₃M (right figure) plotted against vapor bubble height over cell radius at $T = 270$ K. The figures show three different compositions for each mixture, mole fractions of MM is shown respectively by the solid line 25 mol% (—), dashed line 50 mol% (---), and dotted line 75 mol% (⋯).

The average height h of the vapor bubble is estimated by observation of the vapor bubble in the equilibrium cell after loading the mixture in the system and is set at $h = 3$ mm for calculation purposes. Fig. 5 shows the calculated vapor quality for mixtures of MM with MDM, MD₂M, and MD₃M and height $h = 3$ mm at the temperature range used for the measurements of the bubble-points. The vapor quality increases with increasing temperature and again the mixture with a larger fraction of MM shows a steeper increase. For all temperatures and mixtures the vapor quality remains below $q = 8 \times 10^{-4}$.

As shown in Figs. 4 and 5 the vapor quality increase for larger bubble sizes and increasing temperature is small and the assumption is plausible that, by keeping the vapor bubble small, the bubble point of the mixture is measured.

5.2 Uncertainty analysis

The uncertainty is calculated by standardized measurement uncertainty principles²⁰. The expanded uncertainty for the bubble-point measurements is calculated by the root-sum-of-squares method²¹,

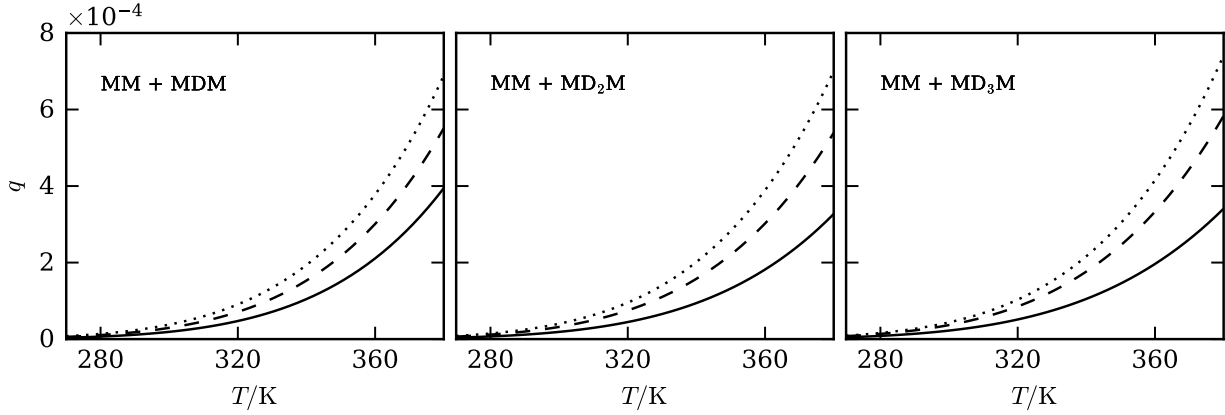


Figure 5: Vapor quality determination on three compositions of each mixture of MM with MDM (left figure), MD₂M (middle figure), and MD₃M (right figure) plotted against temperature with cell radius $r = 22.2$ mm and vapor bubble height $h = 3.0$ mm. The figures show three different compositions for each mixture, mole fractions of MM is shown respectively by the solid line 25 mol% (—), dashed line 50 mol% (---), and dotted line 75 mol% (⋯).

taking into account five principle sources of uncertainty: (i) temperature, (ii) pressure, (iii) sample composition, (iv) loading correction and (v) measurement repeatability.

- (i) *Temperature correction:* The standard platinum resistance thermometer (SPRT) is calibrated regularly. The SPRT was calibrated against the triple points of mercury and water and the freezing point of indium. The standard combined uncertainty in the temperature measurements is determined from the uncertainties in the SPRT, the multimeter to read the SPRT, the calibration, and the possible temperature gradient between the equilibrium cell and the SPRT. The total uncertainty from all sources is estimated to be 0.03 K. A pressure difference is calculated using the thermodynamic model and estimated at the bubble point ($q = 0$) between the experimental measured temperature and 0.03 K from the experimental measured temperature. This pressure difference is taken into account as the temperature uncertainty

$$u_T = P_{\text{calc}}(T = T_{\text{exp}}, q = 0, \bar{z} = \bar{z}_{\text{bulk}}) - P_{\text{calc}}(T = T_{\text{exp}} + 0.03 \text{ K}, q = 0, \bar{z} = \bar{z}_{\text{bulk}}). \quad (1)$$

(ii) *Pressure transducer:* The quartz-crystal pressure transducer (PT) was calibrated with a NIST-traceable piston gauge. The manufacturer stated uncertainty of the PT is 0.01% of the 700 kPa full range. Through regular calibration and temperature control uncertainties of better than those stated by the manufacturer can be achieved. However, a conservative estimate of the pressure uncertainty is used in the overall pressure uncertainty of the bubble-point pressure reported here, namely

$$u_{\text{PT}} = 0.07 \text{ kPa.} \quad (2)$$

(iii) *Sample composition:* The uncertainty in the sample composition is three-fold. First, there is an uncertainty in the gravimetric preparation of the sample. This is reported as the uncertainty in the mole fraction of the components, $u(z_A)$ (for almost pure component #1) and $u(z_B)$ (for almost pure component #2), respectively. The assumption from this uncertainty contribution is that each of the components are pure, with no additional impurities, and that any impurities that might be present have molecular weights similar to the dominant components. Second, there is also a much larger uncertainty contribution that arises from the purity of the components used to form the binary mixture. Though the purities of the pure components as measured by gas chromatography are greater than 99.75% (molar) for all components, uncertainty in bulk composition of component #1 in the mixture (MM in this case) arising from impurity, is still significant. The total uncertainty in the composition of component #1 in the mixture (where the mixture is formed of the almost pure components as well as the impurities and nitrogen) can then be obtained from

$$u(z_1) = \sqrt{(z_{1A}u_{\text{gravimetric}}(z_A))^2 + (z_Au_{\text{purity}}(z_{1A}))^2} \quad (3)$$

in which $u_{\text{gravimetric}}(z_A)$ is the uncertainty of the mole fraction of component A (formed of almost pure component #1) from the gravimetric preparation, $u_{\text{purity}}(z_{1A})$ is mole fraction of the impurity present in the sample (here assumed to be 0.0025 mole fraction as

the worst-case impurity from GC), z_A is the mole fraction of component A, and z_{1A} is the mole fraction of component #1 in component A (as given in Table 1). In this case $z_A u_{\text{purity}}(z_{1A}) \gg z_{1A} u_{\text{gravimetric}}(z_A)$ and the mixture composition uncertainty is dominated by the contribution from the purity.

Finally, there is also an uncertainty in the composition due to entrained air in the mixture, which can have a significant impact on the total uncertainty at low pressures. Because of the low bubble point pressure of the siloxane fluids, the air impurity was found to have a large influence on the uncertainty. To account for the possibility that the degassing of the samples was not complete, a calculation is carried out in order to approximate the air content in the sample, this procedure is described in detail in Section 6.1. As there are no data to represent the effect of air in these mixtures, the partial pressure of nitrogen was used to represent the uncertainty due to air impurities and is calculated as follows:

$$\rho_{\text{N}_2} = \frac{z_{\text{N}_2} n_{\text{total}}}{V_{\text{vessel}}}, \quad (4)$$

$$u_{\text{air}} = P_{\text{N}_2}(T = T_{\text{exp}}, \rho = \rho_{\text{N}_2}), \quad (5)$$

where z_{N_2} is the mole fraction of air impurity. The mole fraction is determined following the procedure in Section 6.1 for all samples. The maximum air impurity estimated of all samples is taken as the air impurity and set at 0.005 mol%. n_{total} is the total number of moles of the mixture and V_{vessel} is the volume of the sample vessel.

- (iv) *Loading correction:* Typically, the equilibrium cell is loaded only one time from a gravimetrically prepared cylinder. In the case in which a second sample is loaded from the same sample vessel, a calculation is performed to account for the uncertainty in sample composition. The composition of the liquid transferred to the cell during the second loading process is calculated by determining the composition of the liquid phase in the sample bottle at ambient temperature (298 K). The difference between the calculated pressure at the reported

bulk composition of the mixture and the pressure at the calculated liquid phase composition determined at the experimental temperature is considered to be the uncertainty due to the reloading procedure and given as follows:

$$\bar{x}_{\text{liquid}} = x(T = 298 \text{ K}, \rho_{298 \text{ K}}, \bar{z} = \bar{z}_{\text{bulk}}), \quad (6)$$

$$P_{\text{liquid}} = P(T = T_{\text{exp}}, q = 0, \bar{z} = \bar{x}_{\text{liquid}}), \quad (7)$$

$$P_{\text{bulk}} = P(T = T_{\text{exp}}, q = 0, \bar{z} = \bar{z}_{\text{bulk}}), \quad (8)$$

$$u_{\text{loading}} = P_{\text{bulk}} - P_{\text{liquid}}. \quad (9)$$

(v) *Repeatability*: The repeatability of the bubble-point measurement is determined as the standard error of the sample mean from the pressures measured during the 15 minutes equilibrium measurement period as described in Section 4. The standard error of the mean is the sample standard deviation divided by the square root of the sample size as²².

$$u_{\text{repeatability}} = \frac{\sigma(P_{\text{measured}})}{\sqrt{n}}. \quad (10)$$

The overall combined uncertainty for each point is calculated by taking the root sum of squares of the pressure equivalents of the temperature correction, pressure transducer, air impurity, loading correction, and repeatability,

$$u(P) = k \sqrt{u_T^2 + u_{\text{PT}}^2 + u_{\text{air}}^2 + u_{\text{loading}}^2 + u_{\text{repeatability}}^2}. \quad (11)$$

The total uncertainty is multiplied by two (coverage factor, $k = 2$) and is reported as the uncertainty in pressure as well as relative uncertainty in percentage for each bubble point measurement. The relative uncertainty is defined as the total uncertainty divided by the measured bubble-point pressure.

6 Experimental results and discussion

Bubble-point measurements were made on three compositions of each mixture of MM with MDM, MD₂M, and MD₃M. In all the mixtures, MM was present in approximately 25 mol%, 50 mol% and 75 mol% of the total mixture. The pressure vs. temperature data for each mixture, as well as the relative pressure uncertainty for each is given in Fig. 6. The tabulated results can be found in the supplementary material. For all of the mixtures, the reported uncertainties are largest for the lowest temperatures (below 320 K). At the lowest temperatures, the pressures are extremely low (below 10 kPa absolute) and, in some cases, below the uncertainty limit of the pressure transducer. Although the uncertainties at low temperatures are high the data are still included here; the data will be weighted differently according to the uncertainty for the fitting of the binary interaction parameters. The only data for binary mixtures of MM + MDM from Abbas¹⁰ is plotted as comparison and good agreement is obtained with the experimental data of this work. A detailed comparison is impossible because of the absence of an uncertainty analysis by Abbas¹⁰.

As seen in Fig. 6 the uncertainties are large for low temperatures. The individual relative uncertainties for the mixture of MM 24.5 mol% + MD₃M 75.5 mol% is plotted in Fig. 7 as an example to observe the impact of the individual uncertainties on the combined uncertainty of Eq. (11). The individual uncertainties do not include the coverage factor ($k = 2$). As can be noticed in Fig. 7, the uncertainty of the air impurity has the largest impact, followed by the uncertainty of the pressure transducer. Because of this large effect of the air impurity a detailed discussion is given in the next section.

6.1 Air impurity

Air impurities and non-condensable gases have a large effect on systems with a low vapor pressure and causing complication for accurate and reliable measurements. To remove air impurities and non-condensable gases the first samples of each mixture of MM with MD₃M were degassed three times, in a similar fashion to the degassing employed by Outcalt and Lemmon²³ and Mansfield

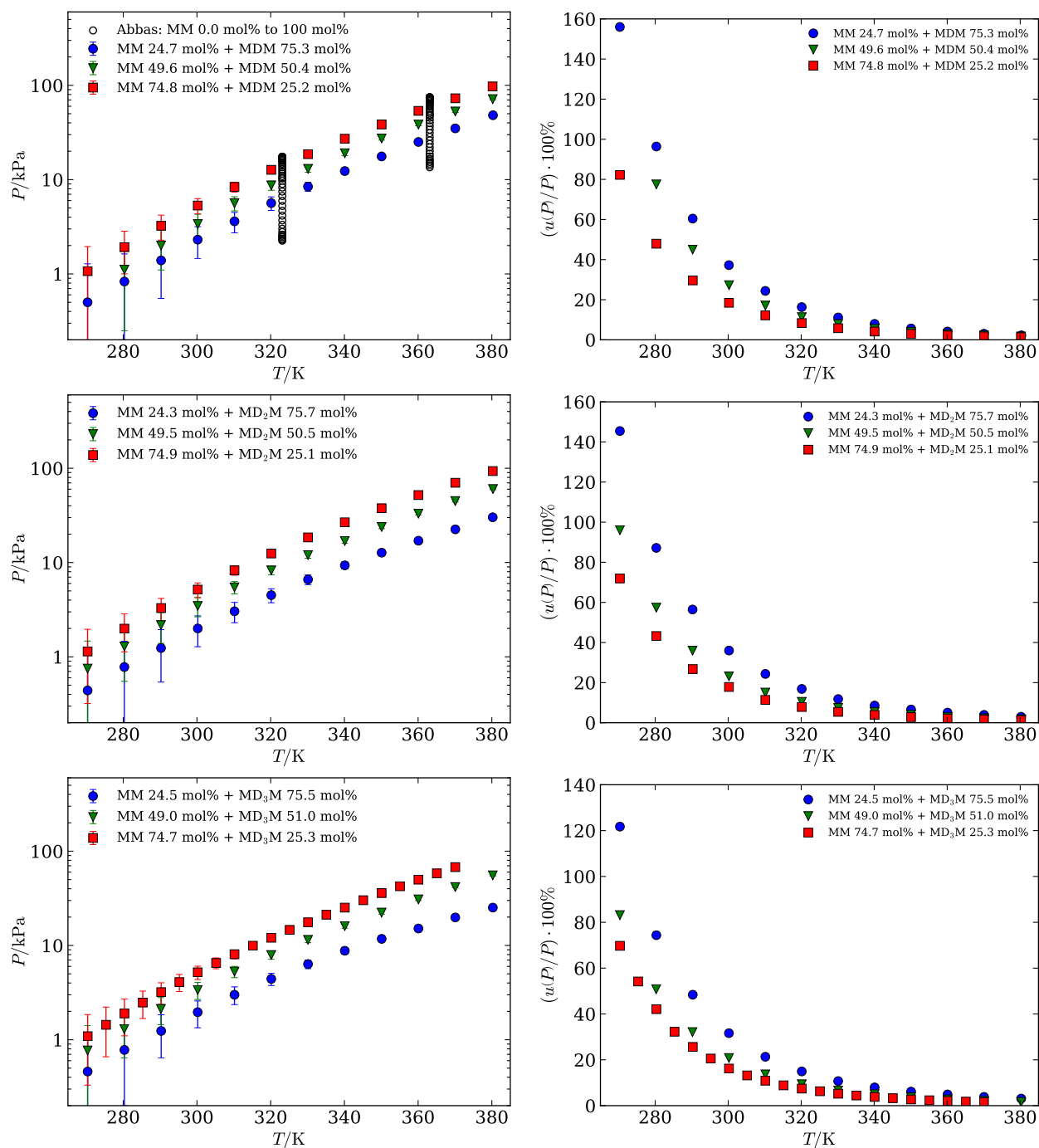


Figure 6: Bubble-point data for binary mixtures composed of MM with MDM (top figure), MD₂M (middle figure), and MD₃M (bottom figure). Left) Pressure vs. temperature data for each mixture composition with experimental data (■, ▼, ●) and literature data from Abbas¹⁰ (○). Right) Relative uncertainty in pressure vs. temperature.

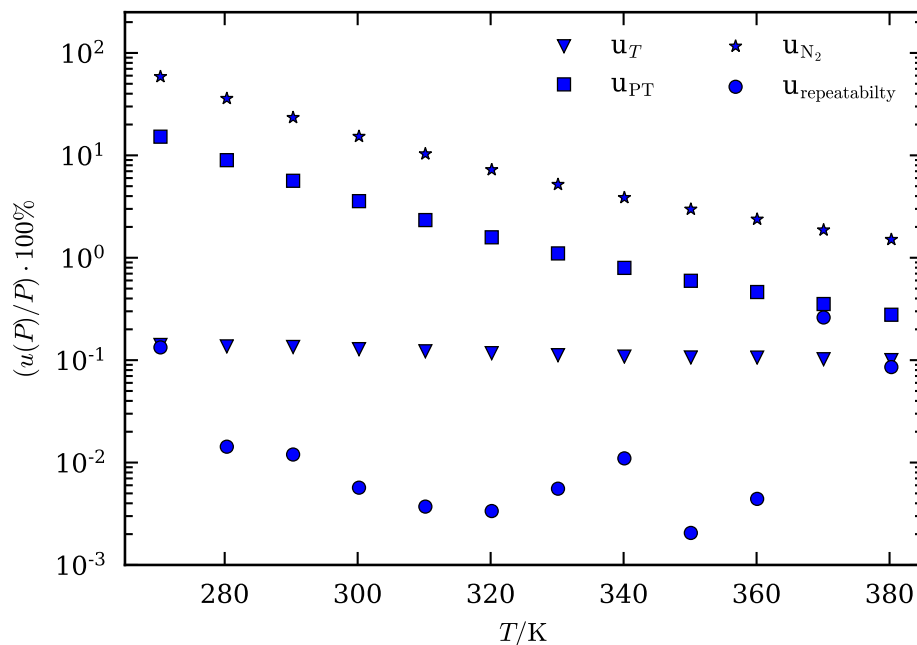


Figure 7: Individual relative uncertainties vs. temperature for the binary mixture MM 24.5 mol% + MD₃M 75.5 mol%.

et al.²⁴. The bubble-point pressures measured of the three times degassed samples show a large deviation from the predicted bubble-point pressure presented in Fig. 8 for a binary mixture of MM with MD₃M with approximately 25 mol%, 50 mol%, and 75 mol% of MM. The final set of samples for binary mixtures of MM and MD₃M was degassed for a minimum of fifteen times and additionally a vacuum was applied to the vapor phase in the equilibrium cell to remove impurities (see Section 6.2). A large decrease in pressure is obtained between degassing three and fifteen times as shown in Fig. 8.

The effect of air on the binary mixtures is qualitatively estimated by fitting the molar composition of nitrogen in a ternary mixture of MM, MD₃M, and N₂ to the measured bubble point pressure at 270 K using the Peng-Robinson equation of state in REFPROP¹⁷ with $k_{ij} = 0$. The molar composition of the ternary mixture is normalized so that the sum of the molar fractions equals one. The normalized molar composition for the ternary mixture of MM, MD₃M, and N₂ is then used to calculate the bubble-point pressures over the range of measured temperatures using the Peng-Robinson equation of state with $k_{ij} = 0$; these results are plotted in Fig. 8. The calculated

bubble-point pressures show good agreement with the measured bubble-point pressures for the samples of all three compositions. Using Peng-Robinson as an estimate, the molar composition of nitrogen decreases by a factor of approximately two orders of magnitude between degassing three and fifteen times from the order of 0.01 mol% to 0.0001 mol%.

Though this is a qualitative estimation of the amount of nitrogen in the sample, it shows the significant impact of N₂ on the bubble-point pressure of the linear siloxanes at low temperatures, which is also confirmed by the high uncertainty shown in Fig. 6. Great care should be taken when measuring fluids with low vapor pressure to ensure the air and non-condensable gases are removed from the system.

6.2 Degassing vapor phase equilibrium cell

Besides the degassing cycles described in Section 4.1, evacuation of the vapor phase in the equilibrium cell is also applied to ensure the removal of non-condensable impurities.

The change in composition of the mixture by evacuating the vapor space of the equilibrium cell has been analyzed using the Peng-Robinson equation of state and a ternary mixture of the binary mixture components and nitrogen. A detailed description of the calculations for the composition and pressure change by degassing the vapor space is given in the supplementary material.

An example of composition and pressure change by evacuating the vapor space is shown in Fig. 9 for a mixture of MM 25 mol%, MDM 75 mol%, and nitrogen impurity taken as 0.005 mol%. The molar composition is normalized so the sum of the molar fractions equals one and is given as \bar{z}_{ini} . The calculations are performed at a temperature of 270 K, a total of 16 evacuation cycles, and the equilibrium cell volume of $V_{cell} = 30$ ml. As seen in the figure the change in composition $\Delta z_i = z_{i,new} - z_{i,ini}$ is on the order of 10^{-5} for all components in the mixture which is on the same order of magnitude as the composition uncertainty of the mixture. The pressure of the mixture decreases proportional to the change of the nitrogen molar fraction and shows an exponential decay with increasing evacuation cycles.

The estimated decrease of pressure by evacuating the vapor phase in the equilibrium cell is

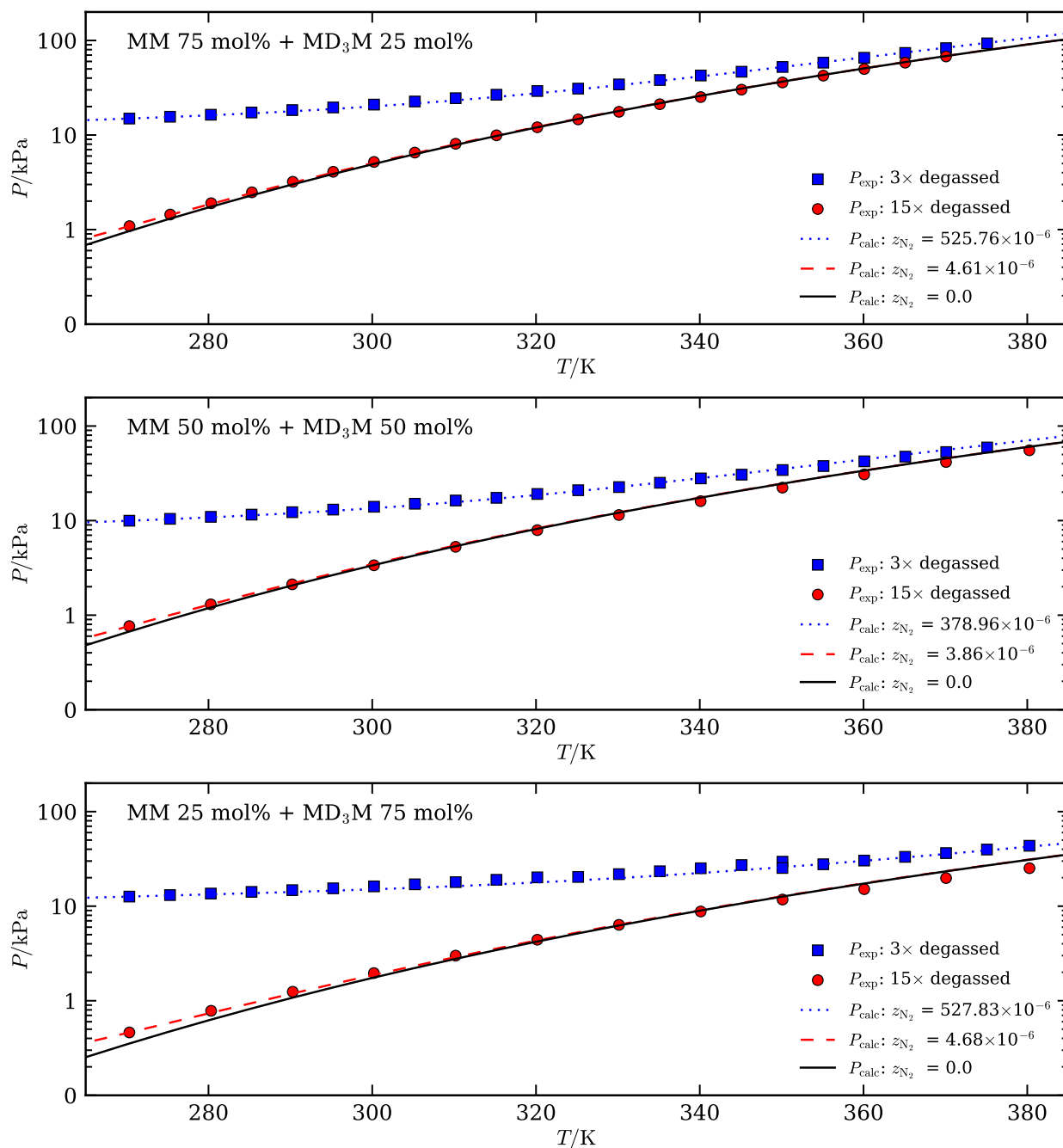


Figure 8: Effect of nitrogen on bubble-point pressure for preliminary experimental results of binary mixtures of MM and MD₃M for three compositions and calculated bubble-point pressures with Peng-Robinson equation of state for ternary mixtures of MM, MD₃M, and nitrogen. Top figure shows MM 75 mol% and MD₃M 25 mol%, middle figure MM 50 mol% and MD₃M 50 mol%, and bottom figure MM 25 mol% and MD₃M 75 mol%. Three times degassed samples are shown with square blue markers (■), fifteen times degassed sampled and evacuation of the vapor space are shown with round red markers (●). The dotted blue line (⋯) estimates three times degassed sample, dashed red line (–) estimates fifteen times degassed sample, and full black line (–) estimates binary mixture of siloxanes without impurities.

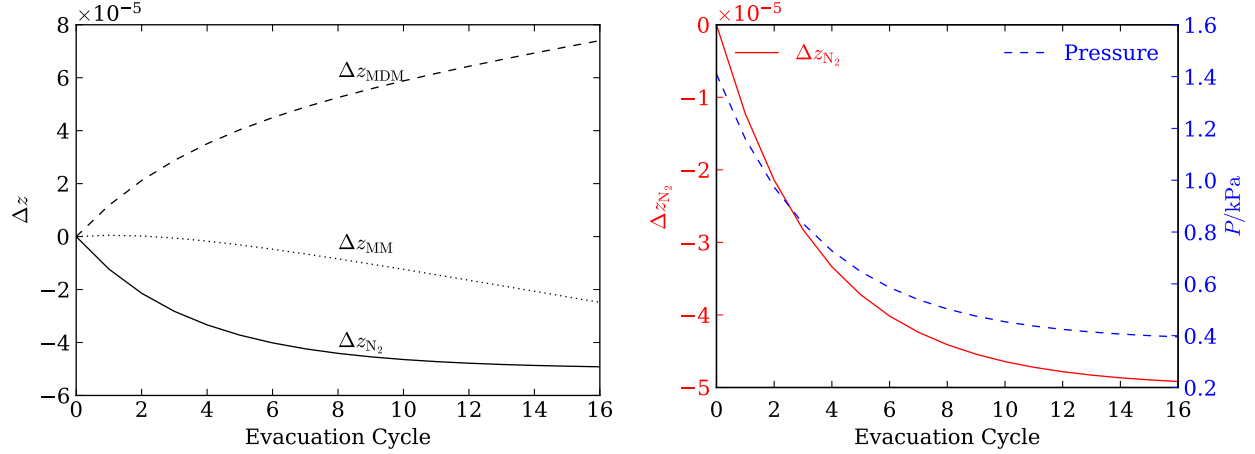


Figure 9: Analysis composition change by evacuating vapor space equilibrium cell. Left) Composition change for mixture of MM 25 mol%, MDM 75 mol% and nitrogen vs. evacuation cycles of the vapor phase. Right) Pressure change and nitrogen molar fraction vs. evacuation cycles of the vapor phase.

compared with experimental data of the evacuation. The initial composition of nitrogen is estimated by fitting the molar fraction of nitrogen in the ternary mixture to the average pressure and temperature of the cell prior to the first evacuation. Following each evacuation the pressure is calculated and compared to the measured pressure. Fig. 10 shows the pressure decrease for the evacuation cycle of two mixtures of MM and MDM and the calculated pressure decrease. It can be observed that the measured pressure also shows an exponential decrease in pressure and qualitative agreement with the calculated pressures.

7 Modeling mixture parameters

The thermodynamic properties of the mixture are modeled in this work using the multiparameter mixture model based on the Helmholtz energy model²⁵. Because it is a Helmholtz based model all thermodynamic properties can be obtained from derivatives of the Helmholtz energy²⁶. The pressure of the mixture can be obtained from

$$P = \rho RT \left[1 + \delta \left(\frac{\partial \alpha^r(\tau, \delta, \bar{z})}{\partial \delta} \right)_{\tau} \right]. \quad (12)$$

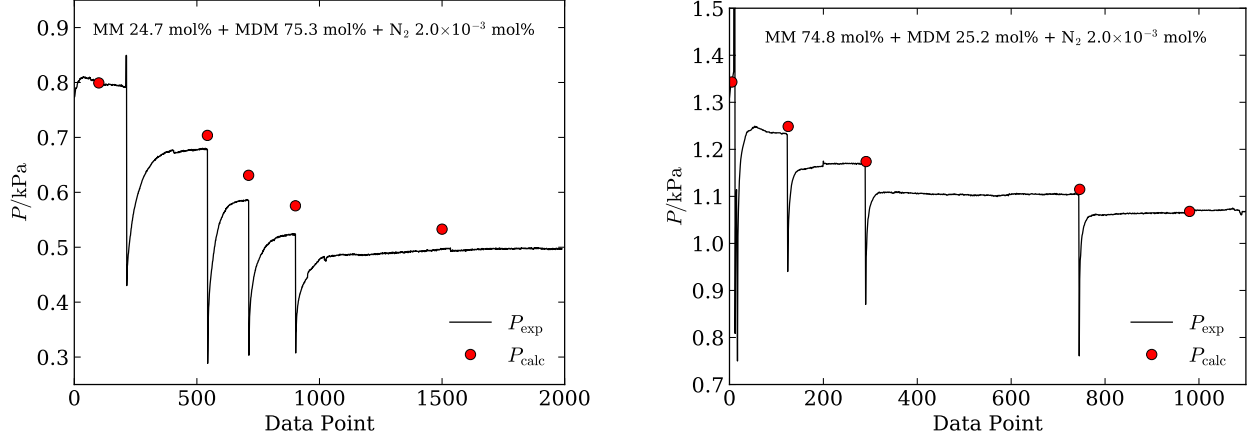


Figure 10: Comparison of measured pressure (P_{exp}) decrease by evacuating vapor space of the equilibrium cell (–) and calculated pressure (P_{calc}) of evacuation cycles (•) for mixtures of MM and MDM. Left) MM 24.7 mol%, MDM 75.3 mol%, and $N_2 2.0 \times 10^{-3}$ mol%. Right) MM 74.8 mol%, MDM 25.2 mol%, and $N_2 2.0 \times 10^{-3}$ mol%.

Other thermodynamic properties like, enthalpy, entropy etc., can be obtained in a similar fashion. The non-dimensional residual Helmholtz energy α^r is expressed in terms of the reduced density $\delta = \rho/\rho_r(\bar{z})$ and reciprocal reduced temperature $\tau = T_r(\bar{z})/T$ where \bar{z} is the bulk composition of the mixture. The reducing parameters $\rho_r(\bar{z})$ and $T_r(\bar{z})$ contain the binary interaction parameters described herein and are fitted for the linear siloxane mixtures.

The binary mixture parameters of the multi-fluid Helmholtz energy equation of state are fitted using the bubble-point measurements given in Section 6. The pure fluids state-of-the-art coefficients for the Helmholtz energy equation of state for MM, MDM, and MD₂M are defined by Thol et al.^{27, 28}, the state-of-the-art coefficients for MD₃M are derived by Thol et al.²⁹.

The reduced mixture parameters τ and δ are calculated through the composition-dependent reducing function for mixture density and temperature. The reducing parameters for the mixture, T_r and $1/\rho_r$ can then be given in common form

$$Y_r(\bar{z}) = \sum_{i=1}^C z_i^2 Y_{c,i} + \sum_{i=1}^{C-1} \sum_{j=i+1}^C 2z_i z_j \frac{z_i + z_j}{\beta_{Y,ij}^2 z_i + z_j} Y_{ij}, \quad (13)$$

where Y represents the parameter of interest, with the parameters T_r and $1/\rho_r$ defined by the ex-

pressions in Table 2.

Table 2: Reducing parameters for Helmholtz energy equation of state.

Y_r	$Y_{c,i}$	$\beta_{Y,ij}$	Y_{ij}
T_r	$T_{c,i}$	$\beta_{T,ij}$	$\beta_{T,ij}\gamma_{T,ij}(T_{c,i}T_{c,j})^{0.5}$
$\frac{1}{\rho_r}$	$\frac{1}{\rho_{c,i}}$	$\beta_{v,ij}$	$\beta_{v,ij}\gamma_{v,ij}\frac{1}{8}\left(\frac{1}{\rho_{c,i}^{1/3}} + \frac{1}{\rho_{c,j}^{1/3}}\right)^3$

The binary mixture parameters $\beta_{v,ij}$, $\gamma_{v,ij}$, $\beta_{T,ij}$, and $\gamma_{T,ij}$ are fitted to experimental data for binary mixtures. These mixture reducing models are weighting functions of the critical properties of the pure fluids that form the mixture based on quadratic mixing rules and the combining rules of Lorentz-Berthelot³⁰. The reducing parameters obey the following relations:

$$\begin{aligned}\gamma_{v,ij} &= \gamma_{v,ji}, & \gamma_{T,ij} &= \gamma_{T,ji}, \\ \beta_{v,ij} &= 1/\beta_{v,ji}, & \beta_{T,ij} &= 1/\beta_{T,ji}.\end{aligned}\tag{14}$$

The γ parameters are symmetric, while the β parameters are not symmetric, so the order of fluids in the binary pair must be handled carefully when implementing the binary interaction parameters.

The binary interaction parameters for binary mixtures of MM with MDM, MD₂M, and MD₃M are fitted. The departure function $\Delta\alpha^F(\delta, \tau, \bar{z})$ is not applied, due to insufficient experimental data to use the departure function. For the fitting of the departure function a relatively large amount of accurate experimental data for thermal and caloric properties is needed (e.g. VLE, homogeneous density, isobaric specific heat, and speed of sound data)³¹. For the fitting, a total of four adjustable binary interaction parameters are considered: $\beta_{v,ij}$, $\gamma_{v,ij}$, $\beta_{T,ij}$, and $\gamma_{T,ij}$. Considering the limited data set available, the parameters fitted here are $\beta_{T,ij}$ and $\gamma_{T,ij}$ because these parameters have the strongest impact on the prediction of the bubble-points and can generally be fit with a relatively small data set. The parameters $\beta_{v,ij}$ and $\gamma_{v,ij}$ are set to unity.

The fitting algorithm developed by Bell and Lemmon²⁶ together with REFPROP¹⁷ are used for the fitting and optimization of the binary interaction parameters for the multi-fluid Helmholtz

energy equation of states. To take into account the uncertainty, which is high at low temperatures as shown in Section 6, the algorithm of Bell and Lemmon²⁶ has been adjusted by weighing the signed error vector using the relative uncertainty. The weighted error vector is calculated as

$$\vec{e}_S = \frac{\vec{P}_{\text{exp}} - \vec{P}_{\text{calc}}}{\vec{P}_{\text{exp}}} \cdot \frac{1}{\vec{u}_{\text{rel}}(P)} \times 100 = \frac{\vec{P}_{\text{exp}} - \vec{P}_{\text{calc}}}{\vec{u}_{\text{exp}}(P)} \times 100, \quad (15)$$

where \vec{P}_{exp} is the measured bubble-point pressure, \vec{P}_{calc} is the calculated bubble-point pressure as a function of the given bubble-point temperature and bulk mole fraction, and $\vec{u}_{\text{rel}} = \vec{u}_{\text{exp}}(P) / \vec{P}_{\text{exp}}$ is the uncertainty of the measured bubble-point pressure. The weighted signed error vector affects the objective function, which is being minimized to find the optimal binary interaction coefficients through the root-sum of squares error metric. By weighing the error vector with the relative uncertainty, points with high uncertainty contribute less to the overall error.

The totality of the available bubble-point data measured in this work is used to fit the binary interaction parameters with the updated optimization approach using the fitting algorithm of Bell and Lemmon²⁶ and weighing the signed error vector using the relative uncertainty as shown in Eq. (15). The fitted binary interaction parameters for the three binary mixtures are listed in Table 3.

Table 3: Binary interaction parameters for multi-fluid Helmholtz energy equation of state.

Mixture	$\beta_{T,ij}$	$\gamma_{T,ij}$	$\beta_{v,ij}$	$\gamma_{v,ij}$
MM + MDM	1.001960	1.007571	1.0	1.0
MM + MD ₂ M	1.003621	1.023157	1.0	1.0
MM + MD ₃ M	0.999076	1.040436	1.0	1.0

The binary interaction parameters are implemented to determine deviations of the measured bubble-point pressure from the equation of state. The results for the binary mixture of MM with MDM, MD₂M, and MD₃M are presented in Fig. 11, where the left figure shows the deviations with estimated parameters by REFPROP (the parameters are estimated because no binary interaction parameters are available for these mixtures) and the right figure the deviation with the newly fitted binary interaction parameters from Table 3.

Deviations from the estimated parameters by REFPROP range from as high as +20% for the

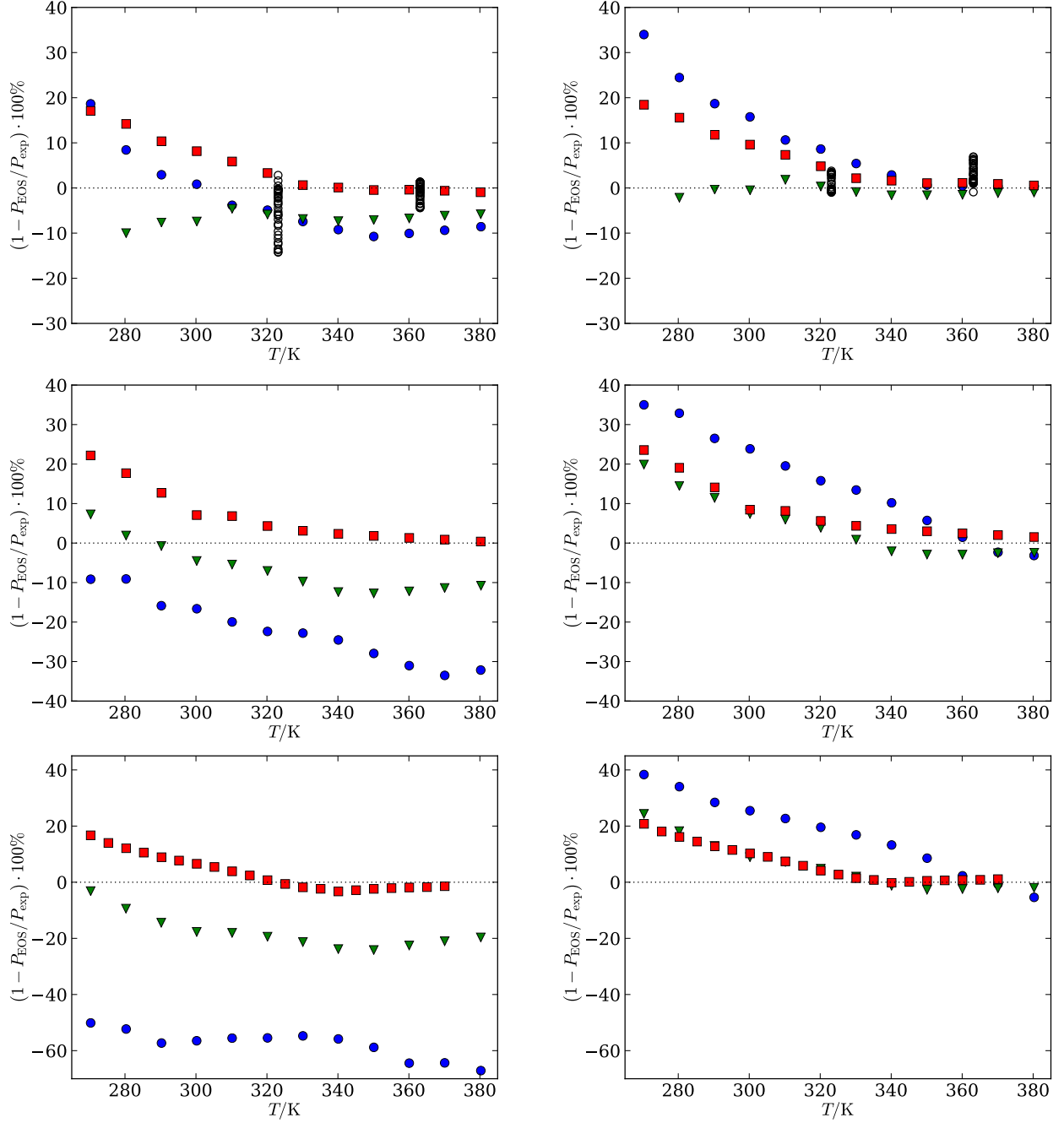


Figure 11: Deviation between experimental and calculated values as a function of temperature of MM with MDM (top figure), MD₂M (middle figure), and MD₃M (bottom figure) for the Helmholtz energy equation of state with experimental data (■, ▼, ●) and literature data from Abbas¹⁰ (○). Left) Estimated binary interaction parameters by REFPROP. Right) Fitted binary interaction parameters listed in Table 3.

low temperatures to -10% for the high temperatures for mixtures of MM and MDM. With the new binary interaction parameters the deviations increased for the low temperatures up to 35%, for high temperatures (above 320 K) the deviations drop to less than 10% for all compositions. The deviation increase at low temperatures is due to the weighing based on the uncertainty introduced in the fitting algorithm, though because of the weighing the deviation at higher temperatures is reduced.

The deviation of MM and MD₂M with the estimated parameters from REFPROP range from +25% to -30% shown in the center left figure of Fig. 11. The new binary interaction parameters presented in the center right figure of Fig. 11 causes again an increase in deviation for low temperatures, but the high temperatures (above 320 K) dropped to less than 10% for all compositions.

For MM and MD₃M the deviation with the estimated parameters are as high as -60% for the mixture with 24.5 mol% MM, the other mixtures deviations range from -20% to +20%. The new binary interaction parameters reduce the deviations for the mixture with 49.0 mol% and 74.9 mol% MM below 10% for temperatures above 320 K. The deviation of the mixture with 24.5 mol% still has a deviation above 20% at 320 K and drops below 10% at 360 K.

7.1 Assessment of physical and extrapolation behavior

The correct physical and extrapolation behavior of the equation of state in regions where no data are available is an essential aspect in the development. This correct behavior is important for pure fluids equation of state as well as multicomponent equations of state. This is because many application require thermodynamic properties outside of the range of validity and thermodynamic properties not investigated experimentally. The diagrams used for the evaluation of the correct physical and extrapolation behavior for the binary mixtures with the fitted binary interaction parameters from Table 3 are shown in Fig. 12 for the binary mixture MM–MDM, Figs. 13 and 14 present the results for MM with MD₂M and MD₃M. All binary mixtures are plotted for a MM molar concentration of 50 mol%. Important for correct physical and extrapolation behavior is that no bumps are present and smooth behavior is observed in the isolines, vapor-liquid equilibrium

curve, and the characteristic ideal curves.

The top left figures show the vapor-liquid equilibrium curve and isobars in the for temperature as a function of specific volume. The selected isobars are plotted from $P_{\min} = 0.5$ MPa to $P_{\max} = 6$ MPa. The vapor-liquid equilibrium curve and isobars are smooth lines up to 800 K, which indicates good physical behavior. The top right figures show the pressure as a function of specific volume and presents the vapor-liquid equilibrium curve and selected isotherms up to $T_{\max} = 1500$ K. Again, no bumps are visible in the isotherms and the vapor-liquid equilibrium curve for all binary mixtures of Figs. 12 to 14. The bottom left figures present the speed of sound as a function of temperature, including the vapor-liquid equilibrium curve and isobars from $P_{\min} = 0.5$ MPa to $P_{\max} = 6$ MPa. The speed of sound of the bubble and dew curve need to have a negative slope and curvature in the vicinity of the critical point, which is the case for all three binary mixtures. The bubble and dew curve merge into a minimum at the critical point, which is also an indication of good physical behavior of the fitted binary interaction parameters and equation of state for the binary mixtures. Further, the isobars show smooth behavior and the extrapolated liquid phase exhibits a negative slope, also indicating good physical and extrapolation behavior. Finally, the characteristic ideal curves are plotted in the bottom right figures. The characteristic ideal curves demonstrate the extrapolation behavior of the equation of state. The characteristic ideal curves are the Ideal curve, Boyle curve, Joule-Thomson curve, and Joule-inversion curve, for more details and definition see Span²⁵, Lemmon and Jacobsen³², Span and Wagner³³. The characteristic ideal curves have to be smooth without any bumps. All characteristic from Figs. 12 to 14 for the binary mixtures show decent behavior. This indicates good extrapolation behavior of the multicomponent Helmholtz energy model with the fitted binary interaction parameters from Table 3.

8 Conclusion

Bubble-point pressures were measured for three binary mixtures of MM with MDM, MD₂M, and MD₃M. For each mixture three compositions were measured with a MM presence in all mixtures of

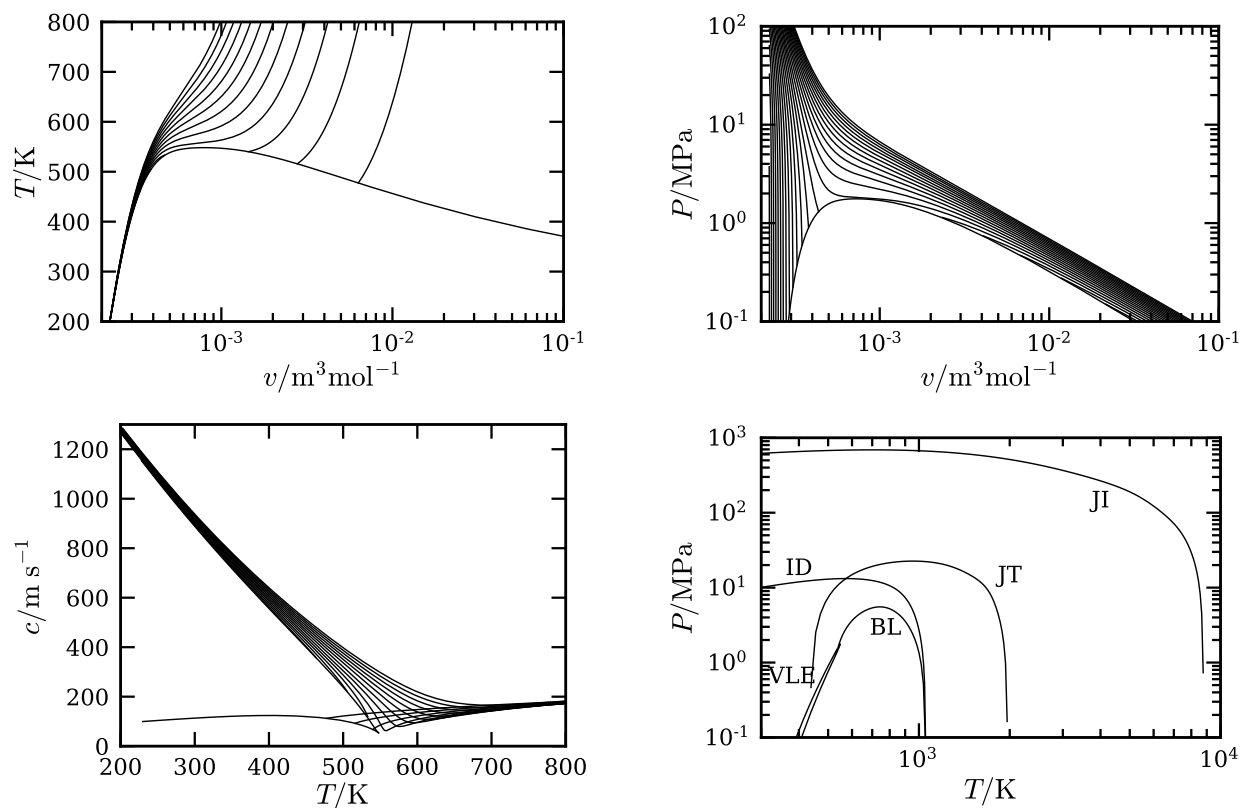


Figure 12: Physical and extrapolation behavior of binary mixture MM–MDM with molar concentration MM of 50 mol%. Generated with the Helmholtz energy equation of state and fitted binary interaction parameters from Table 3. Top left) Temperature as a function of specific volume with selected isobars. Top right) Pressure as a function of specific volume with selected isotherms. Bottom left) Speed of sound as a function of temperature with selected isobars. Bottom right) Characteristic ideal curves JI: Joule-inversion, JT: Joule-Thomson, BL: Boyle, ID: Ideal, VLE: Vapor-liquid equilibrium.

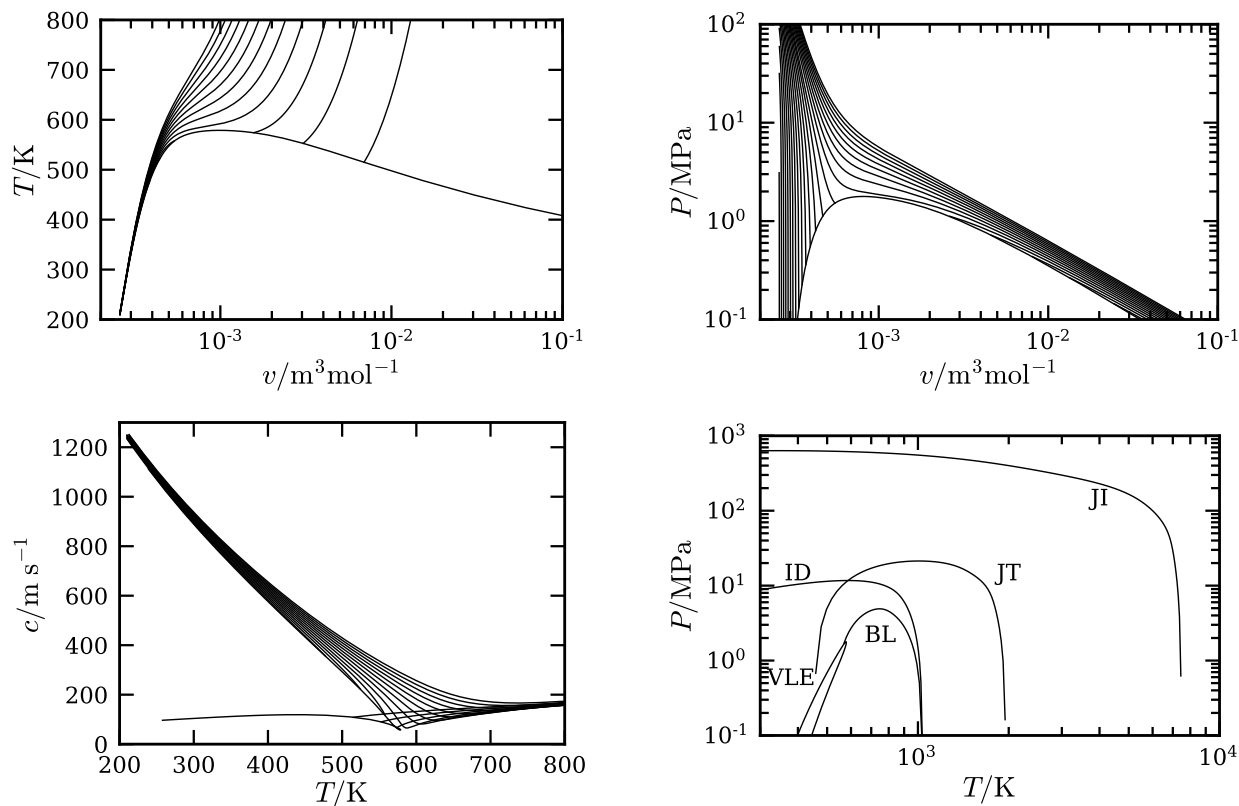


Figure 13: Physical and extrapolation behavior of binary mixture MM–MD₂M with molar concentration MM of 50 mol%. Generated with the Helmholtz energy equation of state and fitted binary interaction parameters from Table 3. Top left) Temperature as a function of specific volume with selected isobars. Top right) Pressure as a function of specific volume with selected isotherms. Bottom left) Speed of sound as a function of temperature with selected isobars. Bottom right) Characteristic ideal curves JI: Joule-inversion, JT: Joule-Thomson, BL: Boyle, ID: Ideal, VLE: Vapor-liquid equilibrium.

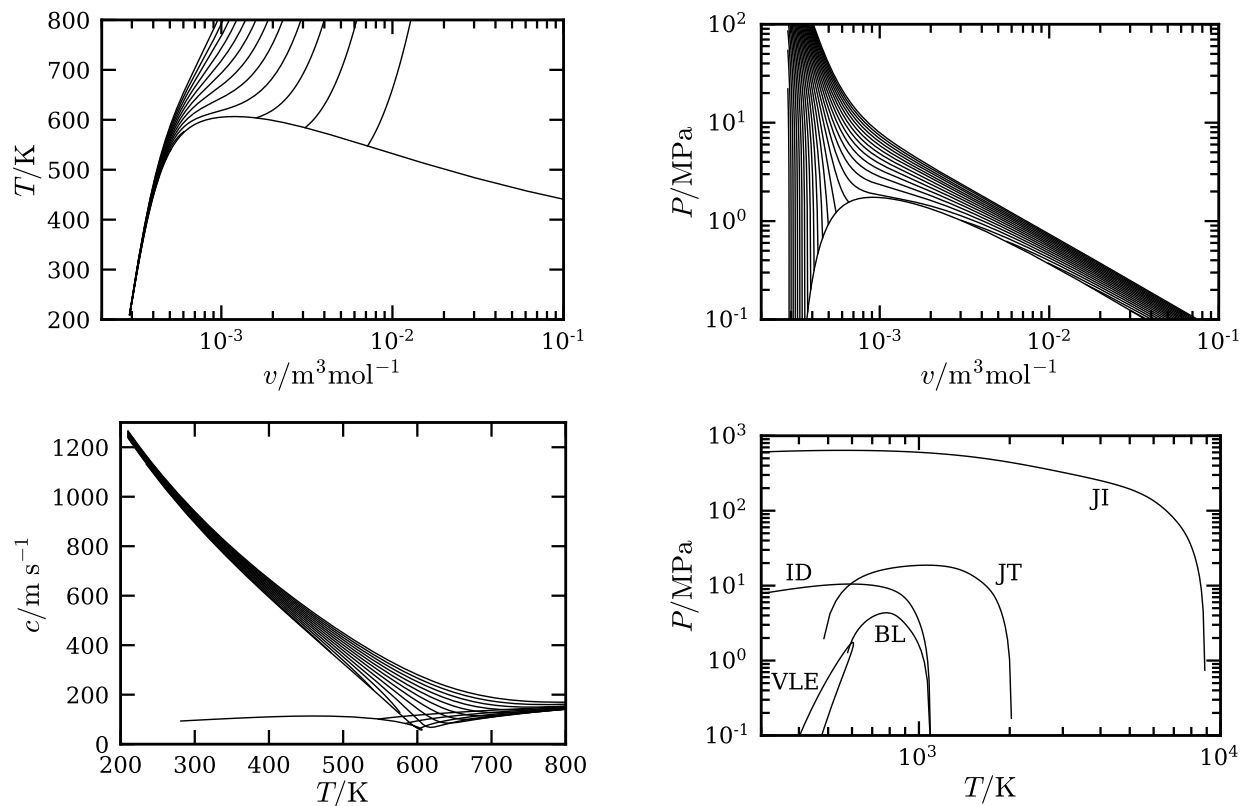


Figure 14: Physical and extrapolation behavior of binary mixture MM–MD₃M with molar concentration MM of 50 mol%. Generated with the Helmholtz energy equation of state and fitted binary interaction parameters from Table 3. Top left) Temperature as a function of specific volume with selected isobars. Top right) Pressure as a function of specific volume with selected isotherms. Bottom left) Speed of sound as a function of temperature with selected isobars. Bottom right) Characteristic ideal curves JI: Joule-inversion, JT: Joule-Thomson, BL: Boyle, ID: Ideal, VLE: Vapor-liquid equilibrium.

approximately 25 mol%, 50 mol%, and 75 mol% of the total mixture. The bubble-point pressures were measured at temperatures from 270 K to 380 K and the pressure ranged from 0.46 kPa to 97.45 kPa for all samples. Large uncertainties are observed for the lowest temperatures (below 320 K) for all binary mixture pairs, as data at these temperatures have very low bubble-point pressures. Though the pressure is below the uncertainty limit of the pressure transducer, the large uncertainty is mostly due to the effect of non-condensable gases in the mixture.

The effect of non-condensable gases was analyzed to determine the impact on the measurements. The analysis was carried out by comparing the bubble-point pressure measurement of a samples degassed for three freezing/evacuating/heating/thawing cycles and samples degassed for fifteen cycles and evacuation of the vapor phase in the equilibrium cell. By estimating the effect of non-condensable gases by fitting a ternary mixture with nitrogen employing the Peng-Robinson equation of state a decrease by a factor of approximately 100 between degassing three and fifteen times is observed from the order 0.01 mol% to 0.0001 mol%. Though this is a qualitative estimation of the amount of non-condensable gases in the sample, it shows the significant impact of nitrogen on the bubble-point pressure of the linear siloxanes at low temperatures, which is also confirmed by the high uncertainty due to air impurities. This also shows the large impact of small amounts of non-condensable gas impurities on fluids with low bubble-point pressure which can affect the thermodynamic properties of the fluid and consequently influence the predicted efficiency and performance of ORCs as well as other processes.

For each binary mixture new binary interaction parameters were fitted for the multi-fluid Helmholtz energy model using the obtained bubble-point pressure data. The fitting was done by weighing the bubble-point pressure data point by the relative uncertainty, which ensures that data points with high uncertainty contribute less to the overall fitting of the binary interaction parameter. At higher temperatures (above 320 K) the new binary interaction parameters represent the experimental bubble-point pressures to within 10% deviation, where previous deviations using estimated binary interaction parameters were of the order of 20%. With exception for binary mixture pair MM–MD₃M with approximately 25 mol% of MM, here deviations up to 20% are observed for

temperatures above 320 K. For temperatures below 320 K, the deviations overall increases, which is due to the weighing based on the relative uncertainty introduced in the fitting algorithm. Furthermore, good physical and extrapolation behavior of the binary mixtures with fitted binary interaction parameters is observed.

9 Funding reporting

The research is partially funded by the European Research Council under Grant ERC Consolidator 2013, project NSHOCK 617603.

10 Associated content

Supporting Information Available

The supporting information is available free of charge.

- Supplement material describing the calculation of the vapor quality in the equilibrium cell.
- Supplement material describing the calculation of the vapor phase degassing in the equilibrium cell.
- Tables of the bubble-point measurement results.

Nomenclature

Roman symbols

c	speed of sound
e	weighted error vector
k	coverage factor
k_{ij}	binary interaction parameter
N	number of components
n	number of moles
P	pressure
q	quality
R	universal gas constant
T	temperature
u	uncertainty
V	volume
z	molar composition
z_{1A}	mole fraction of MM in mixture component A
z_A	mole fraction of mixture component A
Y	reducing parameter

Greek symbols

α	reduced Helmholtz energy
----------	--------------------------

$\beta_{T,ij}$ binary mixture parameter

$\beta_{v,ij}$ binary mixture parameter

ΔY difference in property Y

δ reduced density

$\gamma_{T,ij}$ binary mixture parameter

$\gamma_{v,ij}$ binary mixture parameter

ρ density

σ standard deviation

τ reduced temperature

Sub- and superscripts

i, j component indices

c critical property

calc calculated property

exp experimental property

r reduced property

rel relative property

Abbreviations

EOS equation of state

GC gas chromatography

HRGC high resolution gas chromatography

liq liquid phase

MD₂M decamethyltetrasiloxane

MD₃M dodecamethylpentasiloxane

MDM octamethyltrisiloxane

MM hexamethyldisiloxane

MS mass spectrometry

N₂ nitrogen

NIST National Institute of Standards and Technology

ORC organic Rankine cycle

PID Proportional-Integral-Derivative

PT pressure transducer

PTFE polytetrafluoroethylene

PV pneumatic valve

RTD resistance temperature detector

SPRT standard platinum resistance thermometer

vap vapor phase

VLE vapor-liquid equilibrium

References

- (1) Chirico, R. D.; Frenkel, M.; Magee, J. W.; Diky, V.; Muzny, C. D.; Kazakov, A. F.; Kroenlein, K.; Abdulagatov, I.; Hardin, G. R.; Acree, W. E. et al. Improvement of Quality in Publication of Experimental Thermophysical Property Data: Challenges, Assessment Tools, Global Implementation, and Online Support. *J. Chem. Eng. Data* **2013**, *58*, 2699–2716.
- (2) Fonseca, J. M.; Dohrn, R.; Peper, S. High-pressure fluid-phase equilibria: Experimental methods and systems investigated (2005–2008). *Fluid Phase Equilib.* **2011**, *300*, 1 – 69.
- (3) Narasigadu, C.; Naidoo, P.; Coquelet, C.; Richon, D.; Ramjugernath, D. A novel static analytical apparatus for phase equilibrium measurements. *Fluid Phase Equilib.* **2013**, *338*, 188 – 196.
- (4) Preston-Thomas, H. The International Temperature Scale of 1990 (ITS - 90). *Metrologia* **1990**, *27*, 3 – 10.
- (5) Colonna, P.; Casati, E.; Trapp, C.; Mathijssen, T.; Larjola, J.; Turunen-Saaresti, T.; Uusitalo, A. Organic Rankine Cycle Power Systems: From the Concept to Current Technology, Applications, and an Outlook to the Future. *J. Eng. Gas Turbines Power* **2015**, *137*.
- (6) Wang, M.; Wang, J.; Zhao, Y.; Zhao, P.; Dai, Y. Thermodynamic analysis and optimization of a solar-driven regenerative organic Rankine cycle (ORC) based on flat-plate solar collectors. *Appl. Therm. Eng.* **2013**, *50*, 816–825.
- (7) Meinel, D.; Wieland, C.; Spliethoff, H. Effect and comparison of different working fluids on a two-stage organic rankine cycle (ORC) concept. *Appl. Therm. Eng.* **2014**, *63*, 246–253.
- (8) Franco, A. Power production from a moderate temperature geothermal resource with regenerative Organic Rankine Cycles. *Energy Sustainable Dev.* **2011**, *15*, 411–419.
- (9) Minea, V. Power generation with {ORC} machines using low-grade waste heat or renewable energy. *Appl. Therm. Eng.* **2014**, *69*, 143–154.

- (10) Abbas, R. Anwendung der Gruppenbeitragszustandsgleichung VTPR für die Analyse von reinen Stoffen und Mischungen als Arbeitsmittel in technischen Kreisprozessen. Ph.D. thesis, Technischen Universität Berlin, 2011.
- (11) Kim, S.; Thiessen, P. A.; Bolton, E. E.; Chen, J.; Fu, G.; Gindulyte, A.; Han, L.; He, J.; He, S.; Shoemaker, B. A. et al. PubChem Substance and Compound databases. *Nucleic Acids Res.* **2016**, *44*, D1202–D1213.
- (12) Stein, S. E. NIST/EPA/NIH Mass Spectral Library with Search Program, NIST Standard Reference Database 1A. 1999.
- (13) Wiley Registry of Mass Spectral Data 7th Edition. 2000; <https://www.wiley.com>.
- (14) Outcalt, S. L.; Lee, B. C. A Small-Volume Apparatus for the Measurement of Phase Equilibria. *J. Res. Nat. Inst. Stand. Technol.* **2004**, *109*, 525–531.
- (15) Harris, G. L.; Torres, J. A. *Selected Laboratory and Measurement Practices and Procedures to Support Basic Mass Calibrations*; 2003; Internal Report - 6969.
- (16) Picard, A.; Davis, R. S.; Gläser, M.; Fujii, K. Revised formula for the density of moist air (CIPM-2007). *Metrologia* **2008**, *45*, 149 – 155.
- (17) Lemmon, E. W.; Bell, I. H.; Huber, M. L.; McLinden, M. O. NIST Standard Reference Database 23: Reference Fluid Thermodynamic and Transport Properties - REFPROP, Version 10. 2018.
- (18) Peng, D.-Y.; Robinson, D. B. A new two-constant equation of state. *Ind. Eng. Chem. Fundam.* **1976**, *15*, 59–64.
- (19) Robinson, D. B.; Peng, D.-Y. *The characterization of the heptanes and heavier fractions for the GPA Peng-Robinson programs (Research Report RR-28)*; Gas Processors Association, 1978.

- (20) Joint Committee for Guides in Metrology, *JCGM 100: Evaluation of Measurement Data - Guide to the Expression of Uncertainty in Measurement*; 2008.
- (21) Taylor, B. N.; Kuyatt, C. E. *Guidelines for Evaluating and Expressing the Uncertainty of NIST Measurement Results*; 1994; Technical Note - 1297.
- (22) Everitt, B.; Skron dal, A. *The Cambridge dictionary of statistics*, 4th ed.; Cambridge University Press Cambridge, UK ; New York, 2010.
- (23) Outcalt, S. L.; Lemmon, E. W. Bubble-Point Measurements of Eight Binary Mixtures for Organic Rankine Cycle Applications. *J. Chem. Eng. Data* **2013**, *58*, 1853–1860.
- (24) Mansfield, E.; Bell, I. H.; Outcalt, S. L. Bubble-Point Measurements of n-Propane + n-Decane Binary Mixtures with Comparisons of Binary Mixture Interaction Parameters for Linear Alkanes. *J. Chem. Eng. Data* **2016**, *61*, 2573–2579.
- (25) Span, R. *Multiparameter equations of state: an accurate source of thermodynamic property data*; Springer Verlag: Berlin, Heidelberg, 2000.
- (26) Bell, I. H.; Lemmon, E. W. Automatic Fitting of Binary Interaction Parameters for Multi-fluid Helmholtz-Energy-Explicit Mixture Models. *J. Chem. Eng. Data* **2016**, *61*, 3752–3760.
- (27) Thol, M.; Dubberke, F.; Rutkai, G.; Windmann, T.; Köster, A.; Span, R.; Vrabec, J. Fundamental equation of state correlation for hexamethyldisiloxane based on experimental and molecular simulation data. *Fluid Phase Equilib.* **2016**, *418*, 133 – 151, Special Issue covering the Nineteenth Symposium on Thermophysical Properties.
- (28) Thol, M.; Dubberke, F. H.; Baumhögger, E.; Vrabec, J.; Span, R. Speed of Sound Measurements and Fundamental Equations of State for Octamethyltrisiloxane and Decamethyltetrasiloxane. *J. Chem. Eng. Data* **2017**, *62*, 2633–2648.
- (29) Thol, M.; Baumhoegger, E.; Javed, A.; Span, R.; Vrabec, J. Preliminary equation Helmholtz

equation of state for Dodecamethylpentasiloxane (MD₃M), Personal communication, to be published.

- (30) Leland, T. W.; Chappellear, P. S. The Corresponding States Principle A Review of Current Theory and Practice. *Ind. Eng. Chem.* **1968**, *60*, 15–43.
- (31) Kunz, O.; Wagner, W. The GERG-2008 Wide-Range Equation of State for Natural Gases and Other Mixtures: An Expansion of GERG-2004. *J. Chem. Eng. Data* **2012**, *57*, 3032–3091.
- (32) Lemmon, E. W.; Jacobsen, R. T. A New Functional Form and New Fitting Techniques for Equations of State with Application to Pentafluoroethane (HFC-125). *J. Phys. Chem. Ref. Data* **2005**, *34*, 69–108.
- (33) Span, R.; Wagner, W. On the extrapolation behavior of empirical equations of state. *Int. J. Thermophys.* **1997**, *18*, 1415–1443.

TOC Graphic

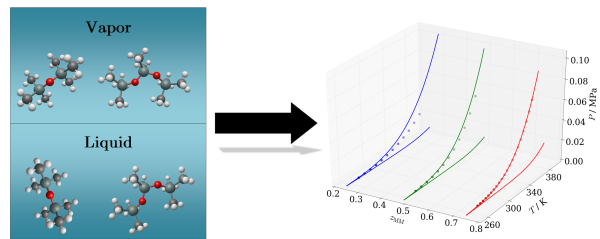


Figure 15: for Table of Contents use only. Title: Bubble-Point Measurements and Modeling of Binary Mixtures of Linear Siloxanes. Authors: Luuc Keulen, Elisabeth Mansfield, Ian H. Bell, Andrea Spinelli, and Alberto Guardone.